American Society of Mechanical Engineers

ASME Accepted Manuscript Repository

Institutional Repository Cover Sheet

Cranfield Collection of E-Research - CERES

ASME Paper Title: On hysteresis in a variable pitch fan transitioning to reverse thrust mode and back

Authors: Dimitrios Vitlaris, David John Rajendran, Richard Tunstall, John Whurr, Vassilios Pachidis

ASME Conf Title: ASME Turbo Expo 2024: Turbomachinery Technical Conference and Exposition

Volume/Issue: _Volume 1: Aircraft Engine _ Date of Publication (VOR* Online): _28 August 2024

ASME Digital Collection URL: https://asmedigitalcollection.asme.org/GT/proceedings/GT2024/87929/V001T01A052/1203753

DOI: https://doi.org/10.1115/GT2024-128701

*VOR (version of record)

Proceedings of the ASME 2024
Turbomachinery Technical Conference and Exposition
GT2024
June 24-28, 2024, London, United Kingdom

GT2024-128701

ON HYSTERESIS IN A VARIABLE PITCH FAN TRANSITIONING TO REVERSE THRUST MODE AND BACK

Dimitrios Vitlaris[1], David John Rajendran[1], Richard Tunstall[2], John Whurr[3], Vassilios Pachidis[1]

[1]Rolls-Royce University Technology Centre, Cranfield University, United Kingdom
[2]Rolls Royce plc., Derby, United Kingdom
[3]Rolls Royce plc., Bristol, United Kingdom

ABSTRACT

A novel hysteresis phenomenon during the transition to and back from the reverse thrust mode in a Variable Pitch Fan (VPF) is identified and characterised in this work. This is done by using a three-dimensional (3D) fully transient Unsteady Reynolds-averaged Navier–Stokes (URANS) with the transitioning fan blade aerofoils simulated by an adaptation of the mesh displacement method. A "real-time" simulation of the complete VPF hysteresis loop is achieved by specifying a blade wall motion through an Eulerian rotation matrix in differential, gradual steps, that is combined with a mesh probe-and-update routine for improved numerical accuracy and stability. The VPF is modelled to be transitioning in a modern 40000 lbf geared high bypass ratio turbofan engine architecture at "Approach Idle" engine power setting in a typical twin-engine airframe with the flaps, slats, and spoilers set for an aircraft touchdown airspeed of 140 knots.

The transition to reverse thrust mode involves flow starvation into the engine, formation of recirculation zones in the bypass duct and the establishment of the reverse stream, all of which occurs in the opposing presence of the free stream flow at aircraft touchdown velocity. The transition back to forward flow mode involves the gradual re-establishment of the free stream which is opposed by the presence of the reverse stream within the engine. It is quantified that in the transition to reverse thrust, the blockage develops with a larger time delay than the disappearance of the blockage during the transition back due to the interplay of the temporal dynamics of fan blade motion and flow field response. The details of the changes in the flow field behaviour, the effect of engine power setting and aircraft touch down velocity on the hysteresis behaviour are explained in detail in the paper. Additional manifestations of the hysteresis phenomena at reverse thrust involving engine spool-up and down, and aircraft acceleration-deceleration manoeuvres are also explored. The hysteresis phenomena described in this work are critical in properly developing control schedules to adapt for potential bi-stable flow field development during the landing run. The study addresses another part of the puzzle in exploring the feasibility of reverse thrust capable VPF engines for future sustainable aircraft to reach aviation climate neutrality.

Keywords: variable pitch fan,VPF hysteresis loop, feasibility study, reverse flow development and dissipation

NOMENCLATURE

Roman characters	
C	Rate of diffusion, constant
$\dot{m}$	Mass flow rate
N	Rotational speed
T	Thrust
Greek characters	
Γ	Stiffness factor
δ	Relative displacement
θ	Rotation angle
ζ	Stagger angle
Subscripts and superscripts	
$disp$	Mesh displacement
ref	Reference value
MTO	Maximum take-off operating point
n	Intermediate fan blade aerofoil position
$stiff$	Mesh stiffness deformation coefficient
z	Axial direction component
Abbreviations	
ADP	Advanced Ducted Propulsor
GCI	Grid Convergence Index
ISA, SL	International Standard Atmosphere, Sea Level
OGV	Outlet Guide Vane
QCSEE	Quiet Clean Short-haul Experimental Engine
URANS	Unsteady Reynolds-averaged Navier-Stokes
VPF	Variable Pitch Fan

1. INTRODUCTION

A Variable Pitch Fan (VPF) can have a twofold functionality in effectively harnessing the benefits of high propulsive efficiency

in modern high bypass ratio turbofan engines and replacing the bulky nacelle-mounted thrust reversal system. As future civil turbofan engines are designed to provide lower specific thrust and thus greater propulsive efficiency, the bypass ratio needs to increase and such engines require low fan pressure ratios to keep the fan power requirement levels reasonable and comply with engine thermodynamic cycle constraints for high overall efficiency. This causes the separation of cruise and take-off working lines to increase and make the fan susceptible to aerodynamic instabilities. In scenarios like these, a VPF can be utilized to ensure the stable operation of the fan at different phases of the flight envelope. Previous research studies have indicated that a VPF can yield significant mission fuel burn benefits in modern high bypass ratio engines [1], [2], [3], [4]. Additionally, when the VPF can be used for reverse thrust generation, it can lead to significant weight savings owing to the removal of the conventional bulky cascade thrust reversers and by paving the way for designing "slim-line" nacelles [5]. Therefore, a reverse thrust capable VPF can play a crucial role in the development of future environment friendly aircraft and aid the civil aviation sector to move closer to NetZero targets [6].

A VPF design allows the rotation of the fan blade to change the stagger angle of the cascade. Reverse thrust can be achieved by rotating the fan blade aerofoils by around 90 degrees through either clockwise ("through-feather" pitch) or anti-clockwise rotation ("through-flat" pitch). This causes the capture throat area of the cascade to shift from the nominal fan inlet to the outlet resulting in the reversal of airflow direction into the fan. Generally, the "through-feather" pitch is preferred because it ensures that there is no entanglement of fan blades and doesn't pose any restrictions on fan blade design in terms of pitch-chord ratio.

The ability of a reverse thrust capable VPF was initially explored by NASA in the Quiet Clean Short-haul Experimental Engine (QCSEE) and the Advanced Ducted Propulsor (ADP) programs. In these programs, experimental isolated rig tests proved the feasibility of VPF designs that can establish reverse thrust in static and limited forward flow conditions [7], [8], [9], [10]. As part of the ADP program, a low noise, low fan pressure ratio reverse thrust capable VPF design was developed that can be adjusted to fit in high bypass ratio engines. Even though there was no information about the reverse flow field in this program, a recent computational study explored the reverse flow characteristics at uninstalled, static and forward flow conditions [11]. Thereafter, the feasibility of using a VPF for reverse thrust applications in realistic installed conditions was addressed in a series of recent publications, which described the reverse thrust flow field, achievable airframe decelerating force levels, distortion levels transferred to the core engine and a design improvement study [12], [13], [14], [15]. All these studies have been carried out at different VPF reverse thrust operating parameters and the key conclusions are: 1) The VPF can generate sufficient airframe decelerating force of up to 45% MTO to aid the aircraft landing run. 2) The circumferential distortion levels into the core engine are manageable for stable core engine operation. The radial distortion levels can be reduced to acceptable levels by rounding the core engine splitter radius to at least 0.1x of the core entry duct height.

A novel method using an adaptation of mesh displacement diffusion equation with small deformation step was developed to study the flow physics in "real-time" during the transition of the VPF from forward to reverse thrust mode at the beginning of the landing run after aircraft touchdown. Several insights into the operational regimes the VPF needs to transition en route to the reverse thrust mode and its implications to engine operability were obtained from this study [16]. However, in certain scenarios of landing, there is a requirement for the VPF aerofoil blades to rotate or flip back to the forward flow position. In the severest of cases, such transition back to forward flow position may occur when the aircraft speed is still high but the engine operates at typical "Approach Idle" power conditions. Such flip back operation may lead to a fan field that is hitherto unexplored in any context. Moreover, the transition back to the nominal operating mode after the transition to reverse thrust mode provides the ability to explore potential 'bi-stable' operating conditions that might arise due to this unique fan hysteresis phenomena resulting from the variation of the fan stagger angle. The recovery process of the VPF from a reverse thrust flow field characterised by large separation zones and adverse pressure gradients is integral to assessing its overall performance. Furthermore, such information on the evolution of flow features as well as the development and subsequently dissipation of reverse flow is crucial on ascertaining the feasibility of engineering a reverse thrust VPF for future high bypass ratio engines.

Therefore, in this work the time-varying flow field evolution while the VPF transitions from nominal forward flow conditions to reverse thrust mode and back to forward flow position is described. The motion of fan blade aerofoils' rotation is achieved by implementing a computational method that uses a wall transfer function to mimic the rotation along with mesh deformation and it is solved in a fully transient URANS framework. The evolution of forward and reverse flow features, decelerating airframe forces, fan power absorption and distortion levels are discussed in the paper and the hysteresis loop is characterised and quantified. The hitherto undescribed fan stagger angle hysteresis, as identified and expounded in this study, provides insights into engine control and operability in both the transition to and from reverse thrust mode.

2. MODEL DESCRIPTION

The new reverse thrust VPF hysteresis loop is examined using an integrated airframe-VPF-engine model with the VPF transitioning from nominal forward flow to the fully reverse thrust mode and back. A 300-seater, twin engine airframe based on the DLR F11 airframe is utilized as a baseline reference [17], [18]. This reference airframe is scaled to accommodate two modern 40,000 lbf two-spool geared turbofan engines with 110 in. fan inlet diameter and a bypass ratio of 14 at cruise. The airframe includes wings, flaps, slats and spoilers in full deployed setting representing an aircraft in landing run. The engine is wrapped in a modern short cowl axisymmetric nacelle, and is attached to a wing via a conventional pylon design at a typical wing chord location selected to optimise installation drag. Full 3D annular geometries of the engine hot and cold flow path are included to capture non-uniformities during flow development. A symmet-

ric half of the airframe with one engine is placed in a cuboidal far field domain where a moving wall is prescribed at the base to represent the rolling runway. The entire airframe-engine-VPF model is shown in Figure 1. Further details about the model development and its usage for VPF reverse thrust studies can be found in [12], [13], [14], [15], [16].

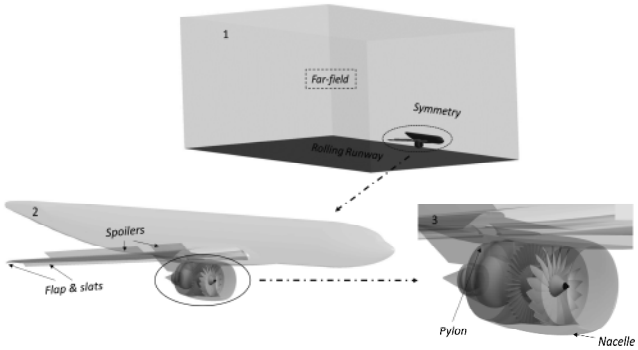


FIGURE 1: Computational domain showing the integrated airframe-engine-VPF model including the engine components [12].

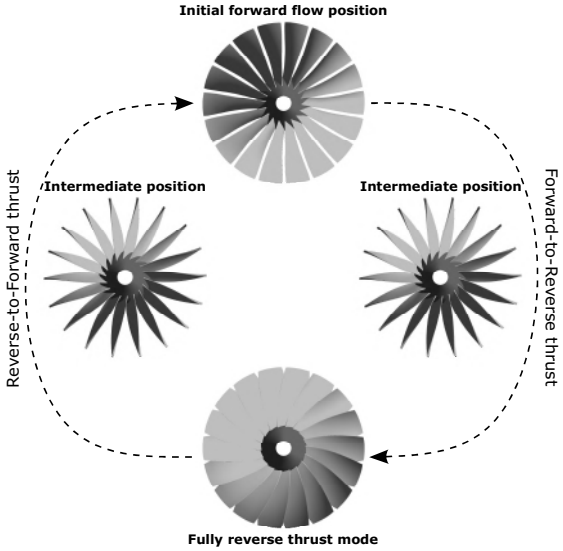


FIGURE 2: VPF blade aerofoils transition from forward flow position to the reverse thrust mode setting and back showing the complete VPF hysteresis loop.

The VPF blade aerofoil design is a scaled version of the 22 inch diameter reverse flow capable ADP fan design developed by NASA [19]. The fan is scaled to 110 inches and has the same flow coefficient as the ADP design but with an extrapolated hub-to-tip ratio from 0.42 to 0.3, which follows the latest high bypass ratio fan design practices. The hysteresis loop is explored by initially rotating the fan blade aerofoils by $\zeta_1{}^o$ through feather pitch reaching the fully reverse thrust setting. $\zeta_1{}^o$ represents a typical reverse flow stagger angle setting within +- 10^o from 90^o of fan stagger angle. After reaching the full reverse thrust setting, the fan blades are rotated back until they reach nominal forward flow position. Figure 2 shows the VPF geometry completing the loop as it transitions from forward flow to reverse thrust mode and back. A novel implementation of the mesh deformation approach that models the motion of the moving fan blade walls transiently as described in detail in [16] and presented here in brief in Section 5 is utilized in this work.

3. COMPUTATIONAL SETUP

A hybrid discretization procedure was followed in which a structured mesh is used in the turbomachinery components of fan rotor, OGV blades and splitter, and unstructured grids are generated for the airframe zones that are external to the engine and the bypass duct. An extensive grid sensitivity study of varying grid sizes was conducted and a mesh of ~50 million elements is finalized. The grid convergence study based on the approach suggested by Roache [20], for local and global parameters of interest, indicated that the finalized grid solution is well within the asymptotic range with the Grid Convergence Index (GCI) values no more than 2%. The dynamic flow field solutions are computed using the compressible, fully transient Unsteady Reynolds-averaged Navier-Stokes equations (URANS) along with the two-equation k-omega SST turbulence model for closure. A commercial fully implicit, finite volume solver, ANSYS CFX, with a bounded second-order-accurate scheme for the spatial discretization and a second-order backward Euler scheme for temporal derivatives is used. Boundary layer flow physics are resolved with explicit grid refinement near the adiabatic no-slip wall surfaces resulting a y+ value of equal or less than one. To capture flow features of varying time scales during the flow development, a meticulous study was conducted to ensure that the time step choice provides adequate resolution to the temporal flow field evolution and establishes robust solver numerics. At each of these timesteps a small, gradual fan aerofoil wall motion that mimics the rotation of the fan blades is imposed. All physical and numerical requirements are achieved by selecting a timestep size that uses 100 time steps to compute 1 complete fan rotation. This leads to having ~0.1^o of VPF blade rotation in every time step eliminating big jumps of blade aerofoil rotation and establishing a near "real-time" simulation of the complete hysteresis loop. Furthermore, 10 inner coefficient loops are found to be sufficient to achieve a converged solution in each time step as equations' residuals are reduced by at least three orders-of-magnitude. Interfaces are introduced to connect various regions of the domain with general grid flux-preserving interfaces between the domains with no relative motion while frozen rotor frame change interfaces are used between the rotating fan domain and the stationary domains of splitter and nacelle intake. This interface method is computationally inexpensive and produces results within 3% variation from the sliding rotor interface, in which the fan rotor domain is physically rotating in the model according to the specified fan rotational speed.

4. BOUNDARY CONDITIONS

In rejected landing scenarios, the VPF rotation from forward flow to reverse thrust mode and back will typically occur at the beginning of the landing run when the aircraft touches down. In such conditions, the engine's power setting is set at "Approach Idle" conditions that are characterized by low fan rotational speed, typically at 40% of the design speed (N_1). Such aircraft considered in this study would typically land at a speed of 140 knots,

therefore this speed is imposed to the ground of the large cuboidal domain to represent the rolling runway. ISA, SL conditions with an atmospheric pressure and a temperature of 288.15 [K] are specified to the far field and a symmetry plane is used for the symmetric half of the aircraft. The modelling of the core engine is carried out by an engine thermodynamic model, which is constructed in the Numerical Propulsion System Simulation (NPSS) framework developed by NASA [21]. This model provides the engine conditions, that correspond to the "Approach Idle" ones, at the core entry duct and core exhaust nozzle. This guarantees that the thermodynamic performance of the core engine is explicitly modelled and is aligned with the integrated model. Using the output from the NPSS model, axial velocity and total temperature are prescribed to the core entry while mass flow rate and total temperature are specified to the inlet of the core exhaust duct. These boundary conditions are selected in such way so that pressure and temperature profiles into the core can be computed by the solver, allowing the investigation of core flow quality and distortion, while the jet from exhaust gases leaving from the engine's exhaust nozzle is represented for overall flow field parameter computations. The engine's "Approach Idle" condition is considered to be the same throughout the VPF hysteresis loop keeping the same fan rotational speed of 40% N_1.

A full VPF rotation from forward flow setting to reverse thrust mode is considered to take 1.5 seconds to complete. This time period is based on the time that conventional propeller pitch-change mechanism takes to be fully actuated and is along the same time scales as the deployment of current cascade thrust reversers. Therefore, the entire VPF rotation loop is considered to take 3 seconds to complete. During the VPF rotation loop, a free body analysis that accounts for airframe decelerating force indicated that the aircraft speed reduces by 5 knots approximately. Previous reverse thrust explorations have shown that such reduction in speed deceleration does not affect the flow physics of the reverse thrust VPF flow field and therefore, in this study the aircraft landing speed is kept the same throughout the 3 second VPF rotation loop.

The VPF hysteresis loop is characterized at 4 fan rotational speeds starting from 40% N_1 with increments of 10 until 70% N_1 at a conventional aircraft touch down speed of 140 knots. This spread of rotational speeds ensures that all possible power settings from "Approach Idle" to typical powered reverse thrust settings for different spool up landing schedules are explored to delineate changes in the hysteresis behaviour. The effect of aircraft landing speed on the hysteresis behaviour is explored at two more typical extended bounds of landing speeds, 120 and 160 knots, at the touch down engine "Approach Idle" setting of 40% N_1. Table 1 shows the conditions considered for the VPF hysteresis loop and the entire solution matrix.

TABLE 1: Solution matrix showing all investigated conditions in this paper.

Parameter	Condition			
Fan stagger angle	0^o to $\zeta_1{}^o$ and back to 0^o			
Fan rotational speed (% of max. *rpm*)	40	50	60	70
Aircraft landing speed (knots)	120,140,160	140	140	140

5. FAN BLADE ROTATION MODELLING

The modelling of the transition of the fan blade aerofoils is based on the mesh displacement methodology that was described by the authors in the transition to reverse thrust mode study [16]. The VPF aerofoils start from the nominal forward flow setting, which is considered as 0^o stagger angle, and transition to the fully reverse thrust setting of $\zeta_1{}^o$ and rotate back to 0^o. 0^o stagger angle setting is referred to as the typical unrotated fan stagger angle position. However, taking into account the optimization of the VPF performance and operability at different phases of the flight envelope, this value may not correspond to the fan stagger angle setting at the on-design point, top of climb or take-off. The stagger angle setting, $\zeta_1{}^o$, corresponds to a typical VPF reverse thrust mode setting and any other angle within +/- 10 degree of this setting may be selected as the preferred reverse thrust setting.

The fan blade aerofoils are physically and dynamically rotated in the domain by imposing a wall motion on the blade walls. The wall motion is prescribed using an Eulerian rotation matrix to provide the new updated location of 0.1^o after each time step, as seen in Eq. 1, and it is applied to each fan blade in its local coordinate system. After the blade walls are rotated to the new location, this motion is transferred to the internal mesh. A displacement diffusion equation, as seen in Eq. 2 and by extension in 3, is used to calculate the motion of the mesh nodes inside the fan passages.

$$\begin{pmatrix} x_n \\ y_n \\ z_n \end{pmatrix} = \begin{pmatrix} cos\theta & sin\theta & 0 \\ -sin\theta & cos\theta & 0 \\ 0 & 0 & 1 \end{pmatrix} \begin{pmatrix} x_{n-1} \\ y_{n-1} \\ z_{n-1} \end{pmatrix} \tag{1}$$

$$\nabla \cdot (\Gamma_{disp} \nabla \delta) = 0 \tag{2}$$

$$\Gamma_{disp} = \left(\frac{\forall_{ref}}{\forall} \right)^{C_{stiff}} \tag{3}$$

The rate of diffusion, C_{stiff}, is computed as 2.85 for controlling the behaviour of dynamic mesh motion in such way so that mesh nodes away from the blade walls absorb the fan blade wall motion with minimum interzonal deformation. Consequently, the elements very close to the walls retain their grid distribution providing sufficient resolution of boundary layer physics throughout the complete VPF transition.

A mesh probe-and-update routine in which mesh quality criteria are probed and examined at each time step is implemented to ensure the grid quality remains high during the entire transition. Whenever a predefined determinant threshold value, that follows turbomachinery mesh quality best practices, is violated, a new mesh is generated in an automatic external routine. The updated high-quality mesh replaces the old grid with similar topology retaining the cell distribution. This ensures that the solution matrix is transferred to the new mesh using a one-to-one zonal approach providing exceptional matching for flux interpolation. After several explorations, it was found that if a new mesh is introduced every 5^o of fan rotation, an aggressive mesh quality threshold can be maintained. The generated grid during the VPF transition at 3 time stamps can be seen in Figure 3.



(a) initial forward flow position **(b) intermediate position** **(c) fully reverse thrust position**

FIGURE 3: Grid evolution showing the mesh deformation depicted at three stagger angles during VPF transition [16].

6. RESULTS AND DISCUSSION

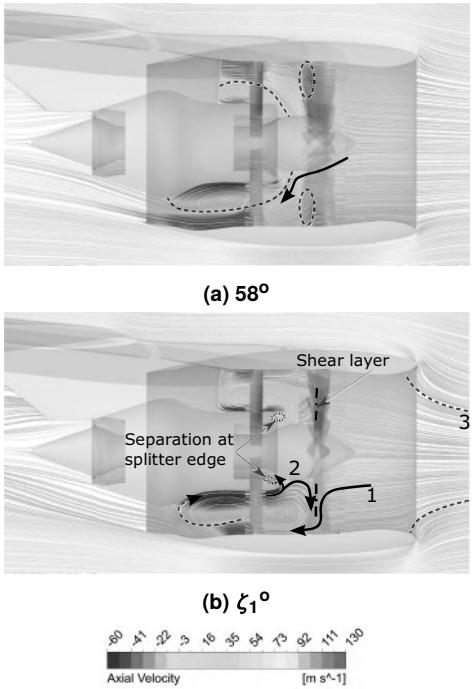
The results are presented in the following order to completely characterize the installed VPF hysteresis loop where the fan transitions from the forward flow position to reverse thrust mode and back.

1. Firstly, the dynamic flow field evolution internal and external to the engine when the fan transitions from forward flow position to the reverse thrust mode is briefly described at a landing speed of 140 knots and the "Approach Idle" engine power setting that corresponds to 40% N_1. Thereafter, the transient flow field evolution during the fan blade rotation from reverse thrust mode back to the initial forward flow position is described to characterize the complete VPF hysteresis loop. The operability of the engine during this loop is examined by computing the total pressure distortion indices at the core duct entry and the resultant airframe forces are also calculated and discussed.

2. The fan flow field development in the hysteresis loop is significantly affected by the fan rotational speed. Therefore, the effect of 4 different fan speeds from 40% N_1 to 70% N_1 is described at a typical aircraft landing speed of 140 knots. Even though, a higher engine power setting than the "Approach Idle" condition is unlikely to occur at the start of the landing run, these rotational speeds are representative of the rotation back to forward thrust that may be required due to rejected landing scenarios taking place when the VPF is spooled up. Moreover, this change in the fan speed and corresponding differences in the hysteresis loop provides insights into the effect of fan power levels for read-across to other designs.

3. The effect of aircraft landing speed on the VPF hysteresis characteristics is described using a constant engine power setting of 40% N_1 and 3 landing speeds of 120, 140 and 160 knots. The additional speeds of 120 and 160 knots are the typical upper and lower bounds of touchdown velocities for conventional aircraft.

4. Two more potential hysteresis scenarios are identified in which the VPF is at the full reverse thrust position in both of them. In the first scenario, the fan rotational speed is the variable that changes and increases from 40% N_1 up to 70% and then drops back to 40% N_1 at a constant 140 knots aircraft landing speed. The other scenario involves the decrease of the aircraft landing speed from 140 to 100 knots and subsequent increase back to 140 knots while the fan rotational speed is kept constant at 40% N_1. This scenario is a numerical investigation that provides insights into hysteresis phenomena driven by the free stream pressure, which acts as a parametric physical surrogate to the landing speed.



(a) 58°

(b) ζ_1°

FIGURE 4: Flow field evolution internal and external to the engine when the VPF transitions to reverse thrust mode [16].

6.1 VPF Blade Transition Hysteresis Loop at at 40% N_1 and 140 knots Aircraft Touchdown Velocity

6.1.1 Flow field evolution during Forward-to-Reverse thrust transition. Figures 4 shows the overall dynamic flow field evolution during the first half of the VPF hysteresis loop, the transition from forward flow position to the reverse thrust mode. Two fan stagger angle settings are used to show the evolution of key flow features internal and external to the engine utilising streamlines on the mid-engine surface. A small increase in mass flow ingested by the fan is noticed in the first 15° due to the more open fan passages. After this, the mass flow keeps decreasing at a close to constant rate with corresponding signatures of flow starvation in the flow path. As the fan reaches the feathered configuration, the fan trailing edge in regions higher than 50% span stalls and large flow separation occurs in the aerofoil passages. This flow separation is noticed in a greater extend at the 58° stagger angle and causes the development of a recirculation region close to the bypass duct hub due to a large radial component of velocity in the fan outlet flow. At this timestamp stagger angle, a shift in the cascade throat area towards the rear of the fan blades has geometrically occurred and the fan is switched to reverse flow mode. Now, the fan suction acts in the nominal fan outlet and bypass regions and this causes the recirculation region inside the bypass duct to further develop and occupy larger volumes. The

free stream, that is pushed further radially outwards in the fan passages, is restricted to the outer annular regions and meets the recirculation zone in a shear layer. The reverse stream emanating from the recirculation zone is strong enough to pass through the OGV blade row. Thereafter, when it arrives at the splitter edge, all of it turns 180^o and feeds the core engine. Finally, at $\zeta_1{}^o$, the reverse stream continues to grow, even less mass flow is ingested and the important flow features are briefly described below:

1. Free stream and reverse stream meet inside the fan passages in a shear layer and both the streams are centrifuged radially outwards.

2. A portion of the reverse stream feeds the core engine while the remaining part escapes and enters the fan rotor where it interacts with the free stream in the shear layer.

3. At the intake, a large drop of ingested axial flow velocity is observed due to the shift of the fan suction to the rear. This causes the stagnation point close to the nacelle lip to move further inwards increasing the spillage flow around the engine and thus enhancing the ground effect.

6.1.2 Flow field evolution for the complete VPF hysteresis loop. The complete VPF hysteresis loop including the fan transition back to forward flow position is discussed in this section. The mass flow rate ingestion trend normalized by the maximum take-off value can be seen in Figure 5 for the complete VPF hysteresis loop. Figure 5a shows how the mass flow rate ingested by the fan varies with time and fan stagger angle. As the fan blades transition to the reverse thrust mode at $\zeta_1{}^o$, the mass flow drops due to the evolution of the flow field features as described in the previous section. Thereafter, the fan blades start to open again transitioning back to the forward flow position in the reverse-to-forward thrust operation. It is observed that, even though the fan blade aerofoils have started rotating back towards 0^o, the ingested mass flow rate keeps decreasing further for the first 3.2^o of fan stagger angle rotation. This corresponds to approximately 0.06 seconds of time delay due to the fan blade transitioning timescale being an order of magnitude higher than the flow field gas dynamic time scales. Alternatively, if at the end of the fan blade transition to reverse thrust, the transition back to forward thrust mode is not initiated but the blades remain at the reverse thrust mode, a flow development time delay of 0.125 seconds to the least mass flow ingestion is noticed [16]. Therefore, this time delay before the mass flow starts increasing during the rotation back to forward thrust mode is a manifestation of the interplay between the temporal dynamics of flow development and fan blade aerofoil movement. As the fan blades keep rotating and the VPF gradually returns to its initial forward flow position, the mass flow rate increases continuously due to the dissipation of separation zones inside the fan and the engine making the flow field to recover to its typical positive axial velocity-dominated forward flow.

The whole VPF hysteresis loop is shown in Figure 5b in which the normalized ingested mass flow rate is plotted against fan stagger angle. The figure shows that there are two ingested mass flow rate values for each fan stagger angle depending upon the path followed to reach the particular setting. The flow ingested

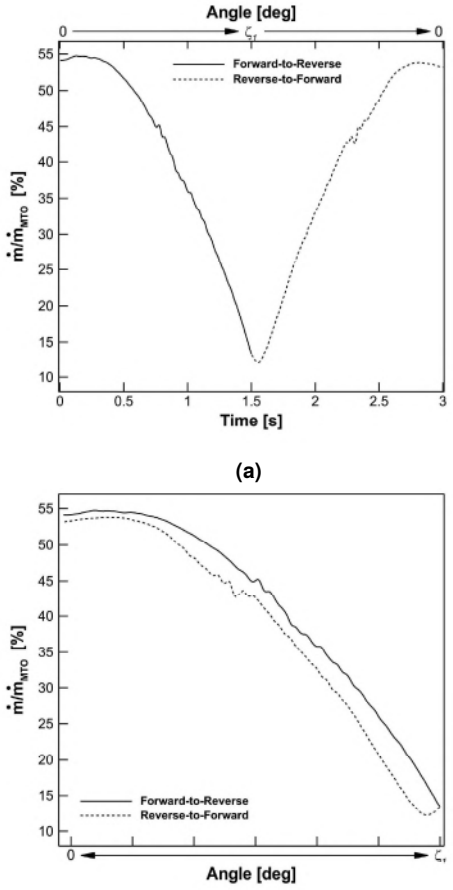
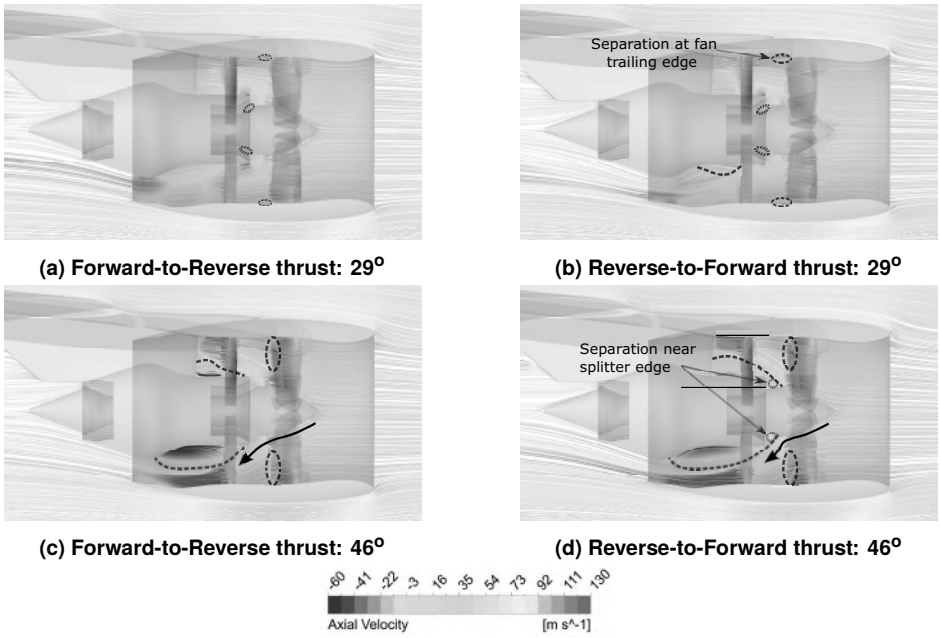


FIGURE 5: Percentage of normalized mass flow rate evolution ingested by the engine. Figure (5a) shows the evolution over time while Figure (5b) shows the VPF hysteresis loop.

by the fan is consistently lower in the reverse-to-forward thrust operation with the biggest difference from the forward-to-reverse thrust operation noticed at the far high end of fan stagger angles near the reverse thrust mode. This is attributed to the fact that, as the fan reaches $\zeta_1{}^o$ and immediately after that starts to rotate back, the flow field takes more time to feel the change in fan stagger angle position and responds with a delay due to transient gas dynamics. At the lower fan stagger angles, the discrepancy of the ingested mass flow becomes less until the VPF reaches approximately 43^o through the reverse-to-forward thrust operation. After this, small perturbations are observed in the mass flow profile, which is an indication of flow feature development inside the engine and is explained by the flow field contours in the next paragraphs. Within 15^o of fan stagger angle rotation near the forward thrust mode, the flow ingested by the fan increases slightly in both operations due to the increased fan passage throat area. A minor difference in mass flows is observed at 0^o, because after reaching this value in the reverse-to-forward rotation, the flow field has not fully developed.



(a) Forward-to-Reverse thrust: 29°

(b) Reverse-to-Forward thrust: 29°

(c) Forward-to-Reverse thrust: 46°

(d) Reverse-to-Forward thrust: 46°

FIGURE 6: Flow field evolution using axial velocity coloured flow streamlines for two timestamp fan stagger angles highlighting the slower dissipation of reverse flow in the reverse-to-forward thrust operation.

The flow field evolution for selected stagger angle settings for both the forward-to-reverse thrust rotation and back is depicted in Figure 6. Because the final conditions of $\zeta_1{}^o$, as seen in Figure 4b, of the forward-to-reverse thrust operation serve as the starting point of the reverse-to-forward thrust operation, two other timestamp stagger angles of 29° and 46° are chosen to show the key development of flow features. These timestamp stagger angles clearly elucidate the differences in the flow field features rather than the minor differences observed in the first few degrees of transition from $\zeta_1{}^o$. The key flow field development in the reverse-to-forward thrust operation is characterised by the presence of the reverse flow at the start of the operation and the gradual and eventual dissipation of this reverse stream and the recovery to forward flow as the VPF transitions to 0 degree.

As the VPF reaches 46° of stagger angle setting in the reverse-to-forward operation, the recirculation zone inside the engine that was formed due to flow starvation has decreased significantly, such that no reverse stream is noticed in the fan domain. This is because, as the VPF recovers, the combination of reduced fan suction acting in the nominal fan outlet and the increased forward flow from the nominal inlet forces back the reverse stream into the engine till it is localized within the bypass duct as a recirculation zone. As the VPF keeps recovering, the radially deflected free stream flow that moves towards the casing inside the fan passages in the reverse thrust mode is observed to recede to its typical axial dominance. The reverse stream-free stream shear layer is pushed out of the fan passages and eventually dissipates. The stalling regions close to the trailing edge of the fan blades are still present, but they continuously reduce in size as the VPF blades rotate to forward flow mode.

At this time stamp, the reverse stream from the recirculation region just manages to feed the core engine. Eventually, the proportion of the core feed flow from the free stream increases. Thereafter, when the core flow is completely fed by the free stream, small perturbations in mass flow occur because of the sudden change in the core ingestion stream. These perturbations are seen in Figure 5b in terms of ingested mass flow and are noticed subsequently as a reduction in the rate of increased ingested flow. The same flow field topology was noticed at 58° of fan stagger angle in the forward-to-reverse thrust operation. Therefore, a range of 12° to 13° difference (corresponding to 0.2 seconds approximately) observed between the two operations can be considered a quantifier for this hysteresis loop.

Thereafter, at 29 degrees, most of the ingested mass flow has been retrieved, and the fan has almost completed its recovery to forward flow mode in that the cascade throat area shifts towards the front of the aerofoil cascade and suction acts in the typical upstream direction. The separating zones at the fan blades trailing edge now occupy a small region close to the fan tip. This causes the flow to move slightly radially outwards from the fan outlet to higher spanwise locations inside the bypass duct. The reverse flow is confined within a small recirculation zone close to the hub of the bypass duct until it eventually dissipates completely. Minor separated flow regions are observed close to the core inlet duct hub because the ingested flow by the fan hasn't fully recovered. This timestamp stagger angle shows the last trace of the reverse flow inside the engine. Contrastingly, in the transition to reverse thrust mode, the reverse stream starts to develop and is noticed much later at 42° of fan stagger angle. Thus, the same range of 12° to 13° discrepancy is observed based on the initial and terminal presence of this recirculating flow inside the bypass duct. Therefore, the dissipation process of the reverse stream takes more time, and it is present for a larger range of fan stagger angles, than its initial creation and development. The delayed gas dynamic response to fan rotation in the reverse to forward transition causes the ingested mass flow to be constantly less throughout the operation

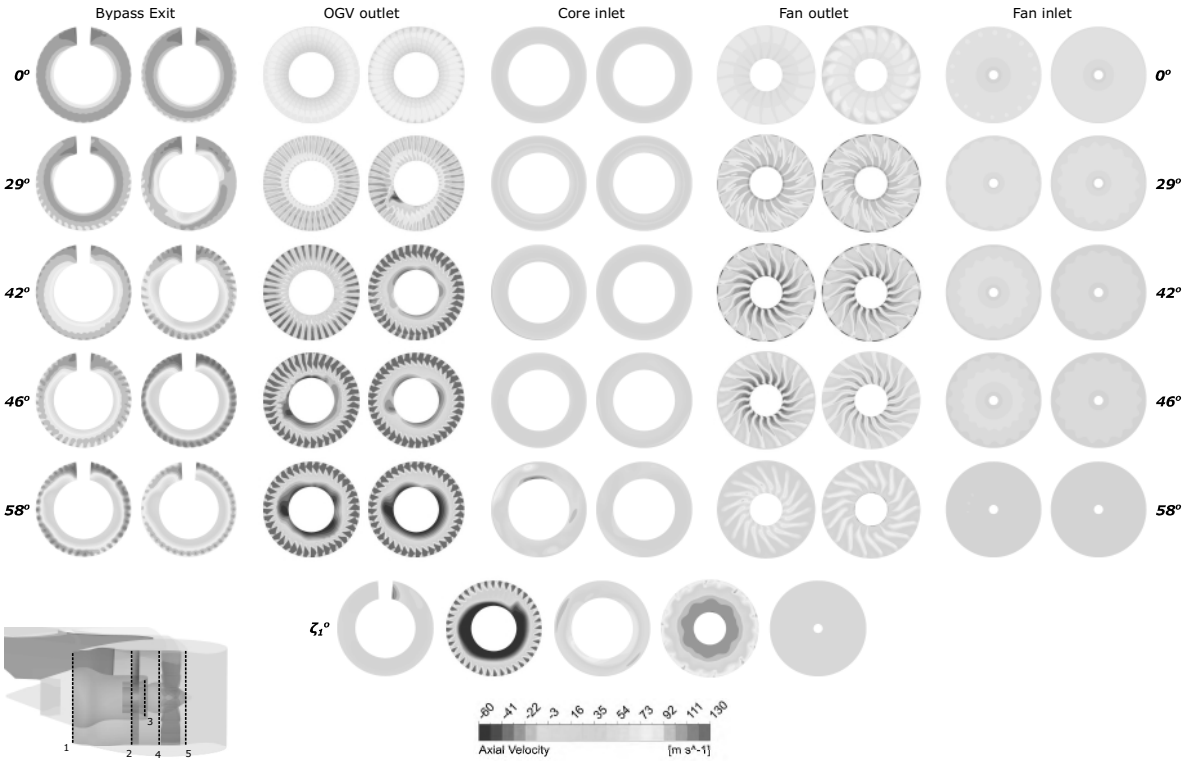


FIGURE 7: Internal flow field development for the complete VPF hysteresis loop using axial velocity contours at five different locations inside the engine for the complete VPF hysteresis loop. The forward-to-reverse thrust operation is represented by the left column at each engine station and the right column shows the reverse-to-forward thrust operation. Core inlet plane is scaled for a more detailed view.

compared to the forward to reverse transition. In the forward to reverse transition, the higher ingested mass flow acts as a deterrent to the development of the reverse flow. On the other hand, in the reverse to forward transition, the lower ingested mass flow acts as an enabler for a longer lasting reverse flow.

The complete development of the flow field for the entire VPF hysteresis loop in the engine internal regions and the fan passages is shown in Figure 7. As the VPF blades rotate to the reverse thrust mode, the recirculation region from which the reverse stream originates develops from 42° of fan stagger angle onwards in regions close to the hub of the bypass duct. This is observed by the negative values of axial velocity in these areas at the OGV and bypass outlets. As this recirculation zone grows bigger, the free stream is centrifuged outwards gaining axial momentum, which occupies the outer annular regions of the bypass duct. The stalling of the fan blades trailing edge starts appearing in the fan outlet from 29° and as the stall region develops and takes over larger portions of the fan, this makes the flow to move towards higher spanwise locations and this flow migration is clearly seen in axial velocity contours at the fan outlet. The presence of the reverse stream in the fan domain is not visible before the 58° of fan rotation, but develops and takes up most of the fan outlet at the fully reverse thrust position, ζ_1°. The fully reverse thrust flow field is exactly the same for both operations. In the reverse to forward transition, this flow field is the initial condition. As the VPF recovers to its initial forward flow position, the slow dissipation of the reverse stream is captured and it is present for a higher range of fan stagger angles. Here, the reverse stream is observed in the fan domain at 58° and occupies a small volume close to the hub. The slower dissipation of the fan stalling is also noticed and the last trace of the reverse flow is seen on the OGV and bypass outlets at 29°. As noticed in this figure, the process of creation, development and destruction of the reverse stream recirculation zone is not circumferentially uniform primarily due to the swirling nature of the flow and the presence of the pylon strut in the bypass duct.

6.1.3 Fan flow field evolution for the complete VPF hysteresis loop. The fan flow field evolution for the entire VPF hysteresis loop is described in more detail for its usage in future design refinement of reverse flow capable designs. The fan flow field is characterised using the spanwise variation of circumferentially averaged axial velocity at the fan inlet and outlet for five different fan stagger angles for both transition rotations, as shown in Figure 8. The differences in the two VPF transition operations can be clearly seen at the fan inlet. As the VPF blades rotate to higher fan stagger angles during the transition to reverse thrust, the axial velocity decreases due to the fan stalling regions initially, until eventually the fan suction shifts towards the rear forcing the reverse stream to enter the fan passages. During the VPF recovery and while the fan blades rotate back, lower inlet axial velocities are noticed because of the extended presence of the reverse flow inside the engine and the delayed response of the dynamic flow field, as reported above. It is emphasized that no reverse flow manages to escape from the fan inlet throughout the VPF hysteresis loop because of the lower "Approach Idle" engine power setting.

In the forward-to-reverse thrust operation, the stalling at the fan tip, indicated by the negative values in Figure 8b, is noticed at 42°. The shift of fan suction in inner annular regions towards the rear of the fan blade aerofoils is observed at 58°. Subsequently, the reverse stream is detected in the fan domain at 75° and enters the fan rotor from locations close to the hub and pushes the free stream towards higher spanwise regions. At ζ_1°, the reverse stream develops further and occupies approximately 60% of the fan outlet.

In the reverse-to-forward thrust operation, the reverse stream takes up more volume at the fan outlet at 75° demonstrating slower dissipation of the stream due to lower free stream mass flow. At 58°, a small portion of that stream is still noticed close to the hub, and as the VPF recovers, the fan suction starts to slowly act in its nominal upstream direction. En route to fan recovery, signatures of the fan tip stall are still observable at 42°. When the fan reaches its forward flow position, the axial velocity profile is noticed to have differences from the initial conditions at the start of the transition to reverse thrust because the flow hasn't been fully developed yet. The difference of stagger angles in both the operations for the appearance of reverse stream in the fan domain is in the range of 12° to 13°.

The evolution of the various flow phenomena inside the VPF passages affects the fan power absorption, as shown in Figure 9. The fan power is calculated using the integral of fan blade torque and rotational speed. In the forward-to-reverse thrust, the fan power increases significantly until it reaches a maximum value of 2x initial forward flow value and starts decreasing after that, but remains at 1.5x forward flow value at the full reverse thrust mode. This is because the stalled fan passages result in a greater power transfer to the flow causing it to reach a peak before the appearance of the reverse stream, which results in a faster drop in the ingested mass flow. The power in the reverse thrust mode still remains higher because of additional losses generated due to the shear layers formed because of free stream-reverse stream interaction that results in a bidirectional flow at the inlet and outlet. The general trend of the power absorption profile in the reverse-to-forward transition is similar to the forward to reverse mode with lower values at each stagger angle due to the lower ingested mass flow and the similar flow field feature development in both the transitions. Even though the power absorption trends are similar, larger differences are noticed at the higher end of fan stagger angles near reverse thrust mode where the flow field takes more time to respond to the fan rotation.

The trends and differences in the power absorption during these operations have implications for the core engine operation. If the fuel flow schedule is defined in such a way as to keep the rotational speed constant throughout the hysteresis loop, the metered fuel flow values in the transition back to forward thrust will be lower than the transition to reverse thrust. Alternatively, if the fuel flow schedules are fixed, the transition to reverse thrust will tend to reduce the fan rotational speed while the transition back to forward thrust will increase it.

6.1.4 Total airframe axial decelerating force. The airframe axial decelerating force during both the transition manoeuvres is obtained using momentum conservation. The near field approach, where the force is computed using the integral

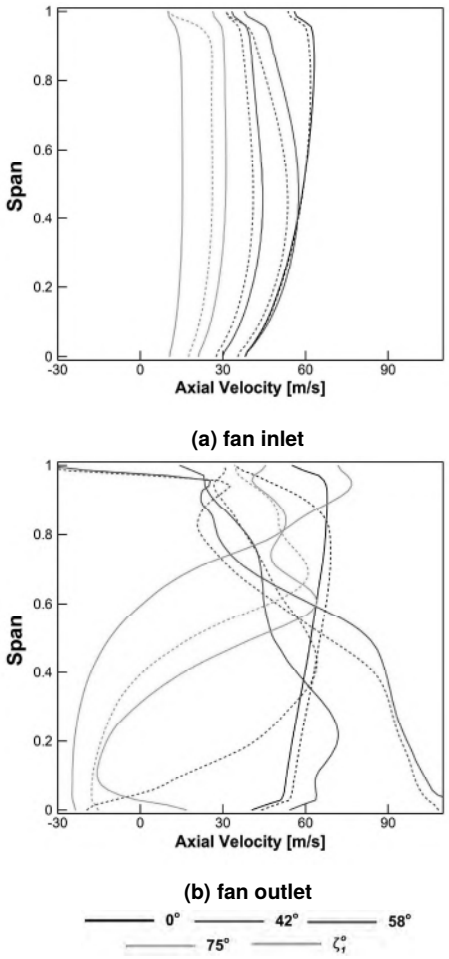


FIGURE 8: Spanwise variation of circumferentially averaged axial velocity at fan inlet (8a) and outlet (8b) for the complete VPF hysteresis loop. The forward-to-reverse thrust operation is depicted by solid lines while dashed lines represent the reverse-to-forward thrust operation.

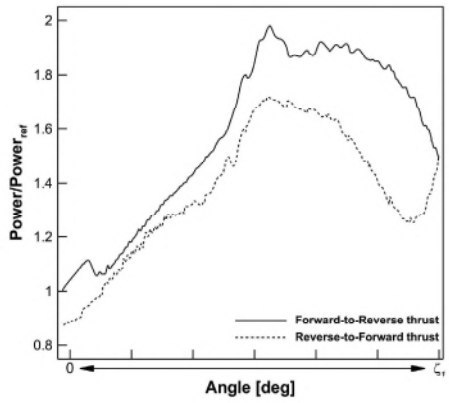


FIGURE 9: Fan power absorption evolution normalised by the nominal forward flow power for the complete VPF hysteresis loop.

of pressure and shear stresses on the entire airframe and engine wetted surfaces, as shown in Eq. 4 is preferred over the far field approach with control volumes due to convection time delay for

flow to reach control surface bounds.

$$F_z = \iint [-pn + \tau.n] dS \quad (4)$$

Where F_z is the resultant axial force, p and τ are the pressure and shear stress terms respectively, n is the unit normal vector to the mesh elements' surface area and S is the total wetted surface area. Further details about the method of force estimation can be found in [15].

Figure 10 shows the time-varying evolution of the resultant axial total decelerating force normalized by the maximum take-off thrust value for the complete VPF hysteresis loop. As expected at aircraft touch down, the decelerating force is zero because the engines produce just enough thrust to overcome the aircraft drag. As the VPF transitions to reverse thrust mode, an initial increase in decelerating force is observed due to the more open fan passages that allow more flow to be ingested. After that, the formation of the separating zone inside the engine causes a drop in bypass duct thrust, which translates to an increase in decelerating force to 12% of T_{MTO} mid-way through. Thereafter, a small drop is noticed again, before it reaches its maximum value of 15% at the end of the operation, because of the time delay that the flow field requires to feel the fan suction that acts in the opposite direction towards the rear. When the VPF transitions from $\zeta_1{}^o$ back to 0^o, initially

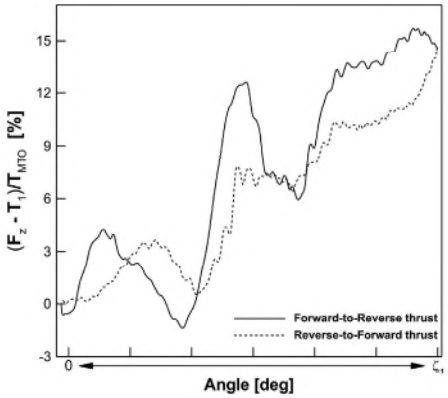


FIGURE 10: Percentage of axial decelerating force evolution normalised by the maximum take-off value for the complete VPF hysteresis loop.

the decelerating force is lower due to the reduction in ingested mass flow. Thereafter, the decelerating force decreases more steadily until it reaches again a point where it stabilizes around 7% of T_{MTO} for a small period of time. This occurs because of the sudden change in the slope of the ingested mass flow by the fan at the feathered position, which is the point of transition for fan suction from the rear towards the front. After this, the engine recovers and more flow is ingested which further decreases the decelerating force. As it nears the 0 degree position, an increase and decrease analogous to the transition to reverse thrust is noticed because of the fan aerofoil movement that causes an increased mass flow from more open passages and the subsequent reduction due to closing passages. The maxima and the minima associated with the dynamics of decelerating force show a similar trend as the reverse thrust transition but the stagger angles at which these occur are shifted to different values that is indicative of the ~12 degrees hysteresis delay explained in the flow field.

6.1.5 Core inlet distortion indices. The core operability that is heavily influenced by the fan power trace is quantified in terms of flow quality using total pressure distortion indices. The circumferential distortion index (CDI) is computed at 5 rings that split the core duct inlet annulus into equal regions, while the radial distortion index (RDI) is calculated for the entire face following SAE S-16 committee standards [22]. The CDI represents the extent of circumferential total pressure depression below the average value for each ring and the RDI represents the radial total pressure depression below the face average. Further details regarding the exact equations can be found in [14].

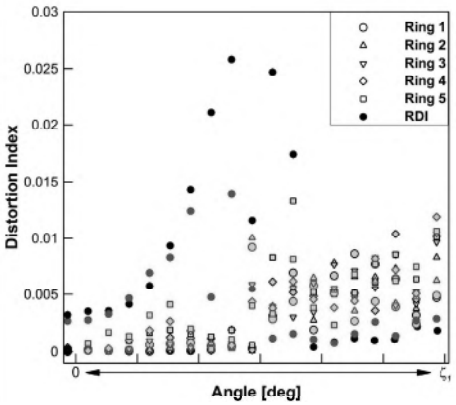


FIGURE 11: CDI and RDI core distortion levels for the complete VPF hysteresis loop. The forward-to-reverse thrust operation is shown in black colour while red colour represents the reverse-to-forward thrust operation.

Both total pressure distortion indices for the complete hysteresis loop are shown in Figure 11. A typical threshold value of 0.07 for these indices, as explained in further detail in [14], is considered as an indicative value, beyond which core engine surge margins will be impacted if the distortion lasts for more than a revolution. During the VPF hysteresis loop, a maximum value of approximately 0.026 in RDI is observed, thus reducing concerns about core engine stability during both the transition manoeuvres. However, it is noted that the peak value during the transition to reverse thrust mode is higher than the transition to forward thrust mode which peaks at 0.015. The lower RDI peak in the transition to forward thrust is attributed to the change of core engine feed flow which transitions from a more distorted reverse stream feed to a cleaner feed from the fan passages. The trends of CDI values are generally similar and significantly away from the threshold for both operations since the circumferential distortions are dominated due to fan swirl and pylon duct pressure non-uniformity in both cases.

6.2 Effect of Fan Rotational Speed on VPF Blade Transition Hysteresis Loop

The effect of fan rotational speed on the hysteresis behaviour is described for three additional values, 50%, 60% and 70% of N_1 in this section. The aircraft landing speed is considered to

be 140 knots and these cases are indicative of the hysteresis loop occurring at higher engine power settings.

The general process of reverse flow development and dissipation during the VPF hysteresis loop, as described for the 40% N_1 condition, is similar at all fan rotational speeds with specific differences arising from the flow fields at the higher powered forward flow starting conditions and reverse flow final conditions. At 50% N_1, the fan reverse flow momentum is high enough to create a blockage to the free stream entering the engine and manages to push it back forming recirculation regions at the nacelle inlet. A further increase in N_1 causes proportional increases in the reverse stream momenta and causes them to escape from the nacelle intake from outer annular regions. First signatures of reverse stream leaving the nacelle intake occur at around 60% N_1.

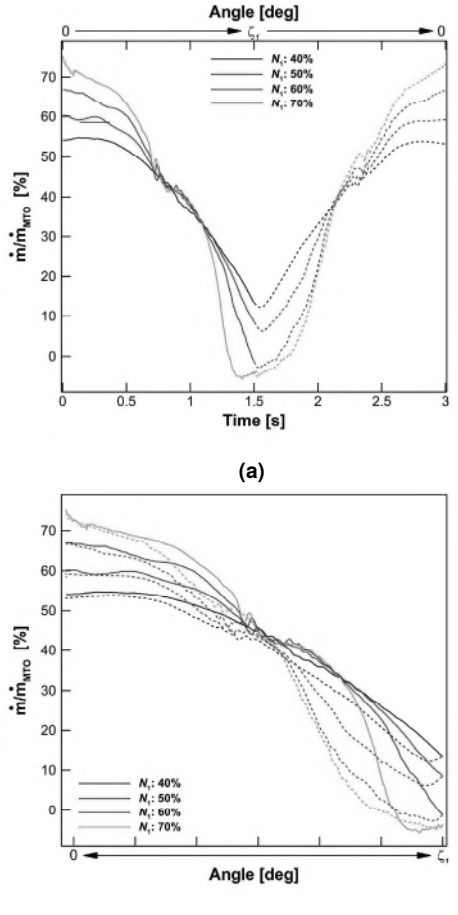


FIGURE 12: Effect of fan rotational speed on the VPF hysteresis loop: Figure (12a) shows the mass flow rate percentage evolution over time while Figure (12b) shows the VPF hysteresis loops. The forward-to-reverse thrust operations are depicted by solid lines while dashed lines represent the reverse-to-forward thrust operations.

The differences in the flow field due to different fan rotational speeds for both the operations are shown using the traces of ingested mass flow in Figure 12. Figure 12a shows the evolution of mass flow normalised by the maximum take-off value against time, while Figure 12b demonstrates the effect of N_1 on the VPF hysteresis loop. As expected, the ingested mass flow at the initial forward flow point is higher with greater fan rotational speeds and as the VFP rotates to $\zeta_1{}^o$, the ingested flow decreases rapidly with slopes that become steeper with rotational speeds. The ingested mass flow trace for all rotational speeds meets at around 43% of $\dot{m}_{MTO}$ for all N_1 cases because the fan passages are completely stalled near the feathered configuration. Thereafter, a significant drop in the mass flow is recorded with higher fan rotational speeds showing steeper reductions on mass flow because the fan suction at the rear of fan blade aerofoils increases with higher N_1. When the VPF is at the fully reverse thrust mode, reverse flow comes out of the intake at the two highest rotational speeds, which is indicated by the negative mass flow values.

TABLE 2: Effect of fan rotational speed: Maximum difference of ingested mass flow rate for the complete hysteresis loop. Fan stagger angle values represent the percentage of the VPF transition to reverse thrust mode.

N_1	$\dot{m}/\dot{m}_{MTO}$	Stagger angle (% of $\zeta_1{}^o$)
40%	6	89
50%	13.1	78
60%	21	75
70%	24.3	73

During the transition back to forward thrust mode, as the reverse stream momentum and amount increases with higher fan rotational speeds, its dissipation inside the engine requires more time leading to bigger differences on mass flow values. As in the transition to reverse thrust mode, the mass flow rates converge in the transition to forward thrust mode as well near the feathered configuration. Thereafter, as the VPF recovers, and more mass flow is ingested, at higher rotational speeds the differences in the mass flow are higher because the larger amount of reverse flow in the bypass duct dissipates slower. Table 2 shows the maximum discrepancy in mass flow rate at fan inlet between the two VPF operations for each fan rotational speed. Typically, the maximum discrepancy increases with higher N_1, especially at higher fan stagger angles, because of the increased reverse stream amount and momentum that requires more time to recede inside the bypass duct until its eventual dissipation. This leads to having larger discrepancy in terms of range of fan stagger angles based on initial and terminal presence of reverse flow inside the bypass duct. Thus, at 50% N_1, this range is between 13^o to 14^o, it increases to 14^o to 15^o at 60% N_1 while the discrepancy ranges between 20^o to 21^o at the highest N_1.

6.3 Effect of Aircraft Landing Speed on VPF Blade Transition Hysteresis Loop

The effect of aircraft landing speed on the hysteresis behaviour is described in this section by considering two more touchdown velocities, 120 and 160 knots, which are typical upper and lower bounds of such aircraft landing speed. The engine is set to the "Approach Idle" condition of 40% N_1 for all three cases.

Figure 13 shows the evolution of ingested mass flow rate at the fan inlet and it is noticed, as could be expected, that generally

TABLE 3: Effect of landing speed: Maximum difference of ingested mass flow rate for the complete hysteresis loop. Fan stagger angle values represent the percentage of the VPF transition to reverse thrust mode.

Landing speed (knots)	$\dot{m}/\dot{m}_{MTO}$	Stagger angle (% of $\zeta_1{}^o$)
120	9.3	81
140	6	89
160	4.9	90

less flow is ingested with lower landing speeds due to lower free stream dynamic head. Thereafter, the temporal transition of fan blades that cause the development and dissipation of the reverse flow regulates the evolution of ingested mass flow rate. Due to the higher free stream momentum at higher aircraft speeds, the time delay for reaching the minimum mass flow rate at the beginning of the transition back to forward thrust mode decreases from 0.065 seconds (4 degrees) at 120 knots to 0.044 seconds (2.8 degrees) at 160 knots. The effect of this decreased time that the flow field takes to feel the change in fan transition direction is clearly noticed in Figure 13b at higher fan stagger angles. Table 3 shows the maximum difference in ingested mass flow for each landing speed and as expected, it increases with lower aircraft landing speeds. Therefore, the range of fan stagger angles in which the reverse flow is noticed inside the bypass duct is 14^o to 15^o at 120 knots and 11^o to 12^o at 160 knots. Other than these differences, the small change of axial velocity at the fan inlet and the difference of time delay periods does not significantly affect the topology of flow feature development and dissipation. Consequently, the fan power absorption, the core distortion indices as well as the axial decelerating force follow the same trend and change proportionally to the dynamic head of the free stream.

6.4 Manifestations of VPF Hysteresis Loop

Two other hitherto unexplored potential manifestations of hysteresis in the reverse thrust VPF have been investigated: 1) Fan rotational speed hysteresis: In this study, the VPF is at the full reverse thrust mode setting and the fan rotational speed increases from 40% N_1 to 70% N_1 and then drops back to 40% N_1 with the landing speed being constant at 140 knots. This can be considered as representative of the spool up-down manoeuvre in the reverse thrust mode. 2) Aircraft landing speed hysteresis: In this study, the VPF is at the full reverse thrust setting of $\zeta_1{}^o$ and is set to the constant "Approach Idle" speed condition, but the aircraft landing speed numerically decreases from 140 knots to 100 knots and then increases back to 140 knots. In this case, the aircraft landing speed is a physical surrogate variable for a hysteresis in the back pressure during VPF reverse thrust operation.

In the fan rotational speed hysteresis loop, the rate of fan speed increase follows a typical slam acceleration profile based on the engine thrust class. The profile was calculated using the transient output of the engine thermodynamic model and subsequently, the core duct inlet and exhaust nozzle conditions in the computational model are updated accordingly for each timestep. The trace of the ingested mass flow during this hysteresis when the VPF is kept at constant $\zeta_1{}^o$ of pitch is shown in Figure 14. As

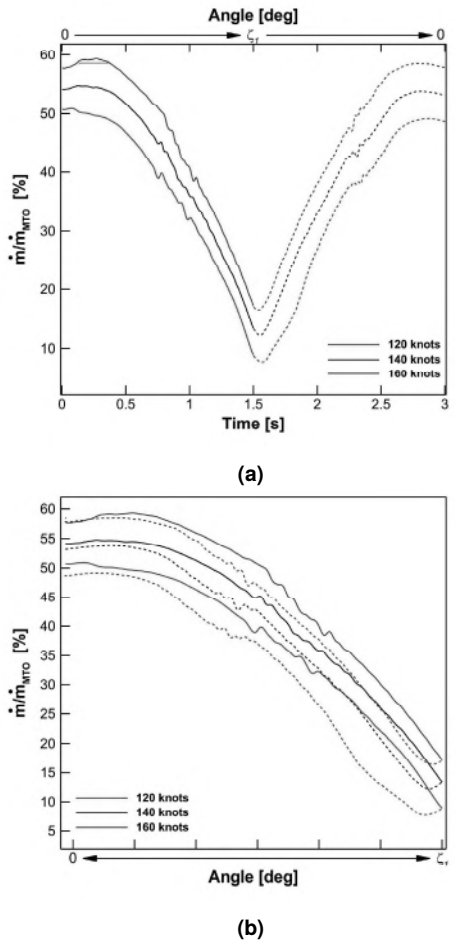


FIGURE 13: Effect of aircraft landing speed on the VPF hysteresis loop: Figure (13a) shows the mass flow rate percentage evolution over time while Figure (13b) shows the VPF hysteresis loops. The forward-to-reverse thrust operations are depicted by solid lines while dashed lines represent the reverse-to-forward thrust operations.

the fan speed increases, the mass flow rate at the inlet decreases because the fan suction at the rear of the fan blades becomes greater and the reverse flow develops until it eventually leaves the engine intake overcoming the free stream momentum at higher than 50% N_1 values. As soon as this reverse stream escapes and disrupts the external flow field, mass flow is ejected out of the nacelle inlet until it reaches its minimum at 70% N_1. When the rotation back to the forward flow mode is initiated, a gas dynamic delay of 0.2% N_1 is observed for the maximum ejected mass flow to start responding to the decrease in N_1. Further, as the fan rotational speed decreases, the external flow field recovers with differences of up to 0.8% of $\dot{m}_{MTO}$ being noticed between the two fan speed change operations in the range of 55% to 70% N_1. The maximum difference in the mass flow is observed at 3% in regions below 50% N_1 because of the slow dissipation of the reverse flow external to the engine. A maximum discrepancy of 4% N_1 is also noticed between the two operations until they reach identical mass flow rates. The external reverse flow eventually disappears and is replaced by the nozzle outflow in a less severe

manner due to the gradual decrease of fan suction towards the back of the engine. The core engine operability as quantified by the distortion indices remain within the threshold for stable operation throughout the loop.

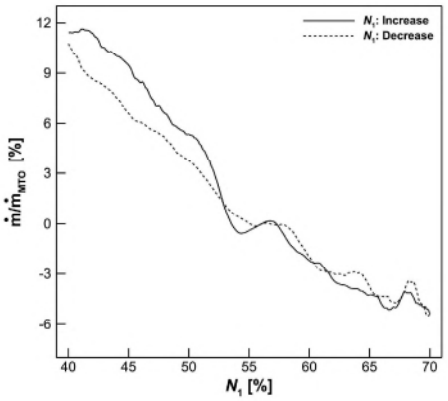


FIGURE 14: Fan rotational speed hysteresis loop: Percentage of mass flow rate evolution ingested by the engine and normalized by the corresponding maximum take-off value.

The aircraft landing speed hysteresis loop where the speed decreases to 100 knots and increases back to 140 knots as the VPF is kept at constant $\zeta_1{}^o$ pitch and 40% of fan rotational seed is shown in Figure 15 in terms of mass flow rate at the fan inlet. The decrease in landing speed causes the free stream momentum to drop and results in lower ingested flows. Higher levels of unsteadiness are observed at the higher landing speeds because of the interaction between the free stream and the reverse stream. At lower speeds, when the free stream momentum reduces, the reverse stream momentum is high enough to overcome the free stream and exit the nacelle intake without strong unsteady interactions. When the landing speed increases back to 140 knots, the mass flow rate at the fan inlet is consistently lower, especially at landing speeds lower than 125 knots. This occurs because the lower free stream momentum at lower landing speeds causes greater fan suction towards the rear developing the reverse stream further. As the free stream starts to gain momentum, the back pressure increases and opposes the development of the reverse stream which leads to lower ingested mass flow. The maximum mass flow rate discrepancy is noticed at 4.7% of $\dot{m}_{MTO}$ at approximately 122 knots while the maximum landing speed difference for both operations to reach the same mass flow at the inlet is computed at 10.5 knots occuring around 4% of $\dot{m}_{MTO}$.

7. CONCLUSIONS

A unique fan hysteresis mechanism that only a reverse flow capable VPF can generate where the fan blades transition back to the nominal forward flow position after the transition to reverse thrust mode is identified and characterised using a novel method that allows the "real-time" physical rotation of fan blades in an installed airframe-engine-VPF model. The effects of fan rotational speed and aircraft landing speed on the VPF blade transition hysteresis loop have been investigated. Additional manifestations of hysteresis phenomena in the VPF reverse thrust setting are explored to provide a complete insight into the temporal dynamics

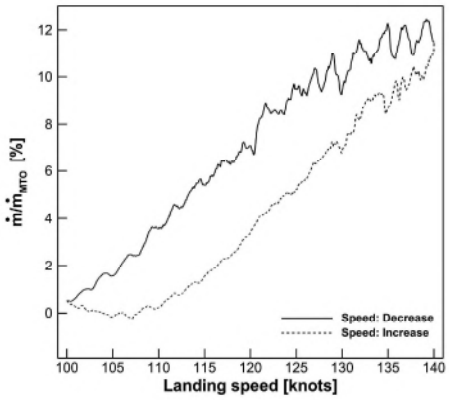


FIGURE 15: Aircraft landing speed hysteresis loop: Percentage of mass flow rate evolution ingested by the engine and normalized by the corresponding maximum take-off value.

of flow development due to cyclic parameter changes beyond the fan aerofoil motion. The key findings from this exploration are:

1. At the typical "Approach Idle" engine power setting, the ingested mass flow throughout the transition back to forward thrust mode is lower due to the slower dissipation of the already existing reverse stream within the engine flow path. On the other hand, during the transition to reverse thrust mode, the formation and development of the reverse stream needs to happen against an already existing free stream flow, which results in larger ingested mass flow and lower blockage throughout the operation. Consequently, depending upon the path of approach, a bi-stable solution exists for the engine ingested mass flow and consequently all other aircraft parameters of interest. The extent of this hysteresis is quantified as a 12-13 degrees difference in the stagger angles between both the transitions for the first appearance and the last disappearance of the reverse flow recirculation zone within the engine.

2. The increase in the engine power setting and fan rotational speed at typical aircraft touch down speeds is observed to result in proportionally larger mass flow differences in the hysteresis loop, albeit with similar stagger angle differences for appearance-disappearance of reverse flow recirculation zones. A study on the effect of typical bounds of aircraft touch-down velocity on the hysteresis loop indicates that at lower landing speeds, larger mass flow differences are observed due to the reduction in the free stream dynamic head that disproportionately affects the recovery back to forward thrust mode.

3. Two other manifestations of the hysteresis loop at the full reverse thrust mode to represent fan spool-up and -down manoeuvre, and numerical aircraft acceleration-deceleration manoeuvre, provide additional insights of other operating variables like fan power and back pressure on the hysteresis behaviour. Both these investigations indicate that the development of reverse flow against opposing free stream results in higher ingested mass flows and lower blockages as compared to the recovery from reverse flow.

The findings from this work in identifying and completely characterising novel hysteresis phenomena are key to successfully engineer reverse thrust capable VPF designs and develop appropriate control schedules that account for this hitherto unknown behaviour. Moreover, the hysteresis loops investigated, are simulations of rejected landing and take-off scenarios during which the VPF needs to navigate these operations and is therefore a step forward in demonstrating the feasibility of using VPF as a thrust reverser for future, sustainable aircraft.

ACKNOWLEDGMENTS

The authors would like to thank Rolls-Royce plc. for supporting this research and for permission to publish the paper.

REFERENCES

[1] Mazzawy, R. S. (ed.). *Performance Study for the Benefits of a Variable Pitch Composite Fan*, Vol. 1: Aircraft Engine; Ceramics; Coal, Biomass and Alternative Fuels; Education; Electric Power; Manufacturing Materials and Metallurgy of *Proceedings of the ASME Turbo Expo 2010: Power for Land, Sea, and Air.* (2010). DOI: 10.1115/GT2010-22148.

[2] Krishnan, G., Perullo, C. and Mavris, D. N. "An Assessment of Relative Technology Benefits of a Variable Pitch Fan and Variable Area Nozzle." 49^{th} *AIAA/ASME/SAE/ASEE Joint Propulsion Conference* (2013): p. 3604. DOI: 10.2514/6.2013-3604.

[3] Denning, R. M. "Variable Pitch Ducted Fans for STOL Transport Aircraft." *Turbo Expo: Power for Land, Sea, and Air*, Vol. 79818: p. V001T01A060. 1972. American Society of Mechanical Engineers.

[4] Halliwell, I. and Justice, K. "Fuel Burn Benefits of a Variable-Pitch Geared Fan Engine." 48^{th} *AIAA/ASME/SAE/ASEE Joint Propulsion Conference and Exhibit*. 2012. American Institute of Aeronautics and Astronautics, Atlanta, Georgia. DOI: 10.2514/6.2012–3912.

[5] McKay, B. and Barlow, A. "The ultrafan engine and aircraft based thrust reversing." 48^{th} *AIAA/ASME/SAE/ASEE Joint Propulsion Conference and Exhibit*: p. 3919. 2012. American Institute of Aeronautics and Astronautics.

[6] Levin, K., Rich, D., Ross, K., Fransen, T. and Elliott, C. "Designing and communicating net-zero targets." On the WWW (2022). Https://www.wri.org/research/designing-and-communicating-net-zero-targets.

[7] Moore, R. D., G. W., Jr. Lewis and Tysl, E. R. "Performance of a low-pressure fan stage with reverse flow." Technical paper. Clevelant, OH. 1976. Report No. NASA-TM-X-3349.

[8] Engineering, Advanced and Department:, Technology Programs. "Quiet Clean Short-Haul Experimental Engine (QCSEE) design rationale." Technical paper. National Aeronautics and Space Administration, Scientific and Technical Information Branch, Washington, DC. 1975. Report No. NASA CR-134842.

[9] Giffin, R. G., McFalls, R. A. and Beacher, B. F. "Quiet Clean Short-Haul Experimental Engine (QCSEE) Design Rationale. Aerodynamic and aeromechanical performance of a 50.8 cm (20 inch) diameter 1.34 PR variable pitch fan with core flow." Technical paper. National Aeronautics and Space Administration, Scientific and Technical Information Branch, Washington, DC. 1977. Report No. NASA-CR-135017.

[10] Levintan, R. M. "Q-Fan demonstrator engine." *Journal of Aircraft* Vol. 12 No. 8 (1975): pp. 658–663.

[11] Williams, T. S. and Hall, C. A. "Reverse Thrust Aerodynamics of Variable Pitch Fans." *Journal of Turbomachinery* Vol. 141 No. 8 (2019): p. 081008. ASME Paper No. GT2018-75739.

[12] Rajendran, D. J. and Pachidis, V. "Fan Flow Field in an Installed Variable Pitch Fan Operating in Reverse Thrust for a Range of Aircraft Landing Speeds." *Journal of Engineering for Gas Turbines and Power* Vol. 141 No. 10 (2019): p. 101018.

[13] Rajendran, D. J. and Pachidis, V. "On the Use of an Inflatable Rubber Lip to Improve the Reverse Thrust Flow Field in a Variable Pitch Fan." *Journal of Engineering for Gas Turbines and Power* Vol. 143 No. 11 (2021): p. 111019.

[14] Rajendran, D. J., Tunstall, R. and Pachidis, V. "Flow Distortion Into the Core Engine for an Installed Variable Pitch Fan in Reverse Thrust Mode." *Journal of Turbomachinery* Vol. 143 No. 7 (2021): p. 071001.

[15] Rajendran, D. J., Tunstall, R. and Pachidis, V. "Estimation of Resultant Airframe Forces for a Variable Pitch Fan Operating in Reverse Thrust Mode." *Journal of Engineering for Gas Turbines and Power* Vol. 144 No. 12 (2022): p. 121017.

[16] Vitlaris, D., Rajendran, D. J., Pachidis, V., Tunstall, R. and Whurr, J. "On the Flow Physics During the Transition of a Variable Pitch Fan From Nominal Operation to Reverse Thrust Mode." *Journal of Engineering for Gas Turbines and Power* Vol. 146 No. 4 (2023): p. 041001.

[17] Rumsey, C. L. and Slotnick, J. P. "Overview and summary of the second AIAA high-lift prediction workshop." *Journal of Aircraft* Vol. 52 No. 4 (2015): pp. 1006–1025.

[18] Rumsey, C. L. "The 2^{nd} AIAA CFD High Lift Prediction Workshop (HiLiftPW-2)." (2013). URL https://hiliftpw.larc.nasa.gov/index-workshop2.html. Accessed Nov. 29, 2023.

[19] Hobbs, D. E., Neubert, R. J., Malmborg, E. W., Philbrick, D. H. and Spear, D. A. "Low Noise Research Fan Stage Design." Technical paper. National Aeronautics and Space Administration, Scientific and Technical Information Branch, Washington, DC. 1995. Report No. NASA-CR-195382.

[20] Roache, P. J., Ghia, K. N. and White, F. M. "Editorial policy statement on the control of numerical accuracy." (1986).

[21] Claus, R. W., Evans, A. L., Lylte, J. K. and Nichols, L. D. "Numerical Propulsion System Simulation." *Computing Systems in Engineering* Vol. 2 No. 4 (1991): pp. 357–364.

[22] Committee, S-16 Turbine Engine Inlet Flow Distortion. *Inlet Total-Pressure-Distortion Considerations for Gas-Turbine Engines* (2017). DOI https://doi.org/10.4271/AIR1419C. URL https://doi.org/10.4271/AIR1419C.



https://dspace.org/

On hysteresis in a variable pitch fan transitioning to reverse thrust mode and back

Vitlaris, Dimitrios; Rajendran, David John; Tunstall, Richard; Whurr, John; Pachidis, Vassilios

2024-06-24
American Society of Mechanical Engineers (ASME)
https://doi.org/10.1115/gt2024-128701
Vitlaris D, Rajendran DJ, Tunstall R, et al., (2024) On hysteresis in a variable pitch fan transitioning to reverse thrust mode and back. In: ASME Turbo Expo 2024: Turbomachinery Technical Conference and Exposition, 24-28 June 2024, London, UK. Proceedings Volume 1: Aircraft Engine

Downloaded from a DSpace repository. https://dspace.org/